Generation of vacancy-interstitial pairs as a possible origin of resistivity switching and ferroelectric properties in $Cd_{1-x}Zn_xTe$

Paweł Jakubas and Piotr Bogusławski
Institute of Physics, Polish Academy of Sciences, 02-668 Warsaw, Poland
(Received 20 June 2007; revised manuscript received 13 May 2008; published 13 June 2008)

Formation of vacancy-interstitial Frenkel pairs, together with the properties of interstitials and vacancies in CdTe, ZnTe, and their alloys were investigated by first-principles calculations. Generation of Frenkel pairs on the cation sublattice strongly depends on the Fermi energy: the presence of excess free electrons reduces the energy barrier for the pair generation from 2.5 eV in intrinsic samples to 1.2 eV. Moreover, E_F determines both the stability of Frenkel pairs with respect to recombination and their binding energy, which varies from ~0.2 to ~1 eV. A strong dependence on the Fermi energy, i.e., on the charge state, is also found for stable sites and barriers for diffusion of isolated interstitials. In particular, neutral interstitials have two (meta)stable sites, corresponding to two local minima of energy, and diffuse by jumps between them. Positively charged interstitials have only one stable site and diffuse by twice longer and curvilinear jumps. For the relevant charge states, the barriers for diffusion range from 0.5 to 1 eV, which imply a high mobility of interstitials. Most of these properties are traced back to the defect-induced deep gap levels, their occupation, and their dependence on the defect's site. The important role of the ionicity of the host is pointed out. On the other hand, generation of Frenkel pairs on the anion sublattice requires energy of about 5 eV, and thus is nonefficient. The obtained results suggest that formation of Frenkel pairs is a microscopic origin of two effects recently observed in Schottky junctions based on CdZnTe and other II–VI alloys, namely, the reversible changes in conductivity by a few orders of magnitude, and the ferroelectric-like behavior of polarization.

DOI: 10.1103/PhysRevB.77.214104 PACS number(s): 61.72.J−, 66.30.Dn, 71.55.−i, 73.61.Ga

I. INTRODUCTION

II–VI compounds, classical semiconductors studied since several decades ago, are currently receiving attention in the context of two applications. First, CdZnTe is the material of choice for energy-dispersive spectroscopy of high-energy radiation such as x rays, gamma rays, and nuclear radiation.[1] The parameter that defines the efficiency of these detectors is the product of two factors, namely, carrier mobility and carrier lifetimes for trapping and recombination. Both factors are largely determined by presence of native defects, as it is discussed in the excellent review by Schlesinger *et al.*[1]

Second, ferroelectrics are potential candidates for applications in nonvolatile memories. The studied materials within this group are organic compounds,[2] as well as perovskite oxides, among which $Pb(Zr_xTi_{1-x})O_3$ has been applied in prototype ferroelectric memories.[3] In this context, the first observation of ferroelectricity in CdZnTe by Weil *et al.*,[4] identified based on ferroelectric hysteretic behavior and dielectric anomaly, suggested the use of these materials in fabrication of memories. These effects have subsequently been observed in CdZnS, CdZnSe, CdMnTe, and CdZnTe alloys,[5–9] but not in the end binary compounds. Recently, ferroelectric effects in CdZnTe have been studied using piezoforce scanning probe microscopy.[10] Nonvolatile gate effect in CdZnTe quantum wells has been demonstrated, which points to a potential new family of nanoscale one-transistor memories.[10] Moreover, these materials exhibit conductivity switching, i.e., reversible changes between states in which conductivities differ by a few orders of magnitude.[5–8,11] The effect is induced by large external voltage and may be utilized in memory applications. A more detailed summary of experimental data is given in Sec. VIII.

Substantial experimental progress was not paralleled by theoretical understanding of the effects above. Previous attempts to elucidate the origin of ferroelectricity include the hypothesis that the effect in bulk CdZnTe is related to the rhombohedral distortion of the zinc-blende structure,[12] as the high symmetry of zinc blende does not allow for the ferroelectricity. However, this hypothesis was disproved by recent experiments.[13] Changes in electric polarization may be induced by structural instabilities at the atomic level. This possibility was suggested in Ref. 14, but the results of this study were nonconclusive, as it is discussed below. The problem of resistive switching in CdZnTe has not been addressed theoretically so far to the best knowledge of the authors.

To get an insight into the possible microscopic origin of resistive switching and ferroelectric effects, we study the formation of vacancy-interstitial (*V-I*) Frenkel pairs (FPs) as well as the properties of isolated vacancies and interstitials by using first-principles calculations. The presence of high external voltages in the diodes is taken into account by varying the Fermi energy, which allows studying of the impact of excess free carriers on generation of *V-I* pairs. The results reveal the important influence of the Fermi energy on generation and stability of the FPs. As it was mentioned above, polarization effects are not observed in pure CdTe. This indicates that the phenomenon is associated with the presence of Zn ions in CdZnTe alloy. Consequently, defects related with Zn in CdZnTe, i.e., Zn interstitials, Zn_i, and V_{cation}-Zn_i pairs, are analyzed in detail. Formation of defects on the anion sublattice is shown to be nonefficient. Diffusion of cation interstitials in CdTe and ZnTe, which has not been previously analyzed by theory in detail, is found to be operative because of the small energy barriers, but the character of jumps between stable sites depends on the charge state of

interstitials. Moreover, most of the properties of interstitials can be explained by the dependence of their electronic structure on the location in the unit cell. Results for vacancies, investigated previously,[15–17] are included for the sake of completeness and consistency of the paper.

The obtained results allow proposal of a qualitative explanation of a number of experimental results for CdZnTe on resistivity switching and ferroelectric-like behavior. CdZnTe may be considered as a typical or prototype alloy, and thus the conclusions may be extended to other II–VI alloys in which similar behavior has been observed. Finally, the studied properties of native defects in CdZnTe are relevant also for the detectors of nuclear radiation.

The paper is organized as follows: In Sec. II technical details are given. Sections III and IV present results for isolated vacancies and interstitials, respectively, and compare the results with those obtained in previous studies.[15–17] Next, in Sec. V we study the diffusion of interstitials in CdTe and ZnTe. In Sec. VI, the influence of growth conditions on the formation of point defects is briefly pointed out. The formation and stability of vacancy-interstitial pairs in CdTe and ZnTe are analyzed in Sec. VII. In Sec. VIII we summarize the experimental data and propose their tentative microscopic explanation based on the obtained results. Finally, Sec. IX summarizes the paper.

II. COMPUTATIONAL TECHNIQUE

The calculations have been performed using density-functional theory (DFT) (Refs. 18 and 19) in generalized gradient approximation (GGA).[20,21] The numerical implementation in the QUANTUM-ESPRESSO code[22] uses ultrasoft Vanderbilt pseudopotentials[23,24] and plane waves as the basis set. The Methfessel–Paxton smearing method[25] has been used for obtaining partial occupancies. The width of smearing has been chosen to be 0.272 eV. The cut-off energies of 408 eV for the plane waves' expansion and 1632 eV for the electronic charge density have been found to be sufficient in all studied cases to obtain convergent results. Ionic positions have been optimized until the forces acting on ions were smaller than 0.026 eV/Å. Large unit cells with 64 atoms have been employed. Thus, substitution of one Cd atom by Zn corresponds to the alloy containing 3.1% of Zn, etc. Brillouin-zone summations have been performed using the Monkhorst–Pack scheme[26] with a $2\times2\times2$ k-point mesh. The calculations do not include spin-orbit interaction.

The climbing nudged-elastic-band (NEB) method[27] was used to calculate minimum-energy pathways and energy barriers for both the interstitial diffusion and formation of FPs. Five (for interstitials) and seven (for FPs) intermediate configurations (replicas) were chosen between the two stable configurations. The computations were done with the parameters given above. The forces in each replica were computed with the stop criterion fixed at 0.026 eV/Å. Due to the optimization with the direct inversion in the iterative subspace (DIIS) algorithm[28] applied to the replica with the highest energy, the errors on barriers at saddle points are similar to those at the stable states.

Bulk Cd and Zn metals crystallize in the hexagonal-close-packed (hcp) structure. Lattice parameters have been found with $16\times16\times16$ Monkhorst-Pack sampling. The results for Cd (a=3.030 Å, c=5.752 Å) agree with experiment[29] (a=2.98 Å, c=5.62 Å), and the results for Zn (a=2.657 Å, c=4.963 Å) are even closer to the experimental values[29] (a=2.66 Å, c=4.95 Å). Bulk Te crystallizes in the γ Se trigonal structure (space group $P3_121$, no. 152). The calculated lattice parameters are a=4.64 Å, c=6.01 Å, and u=0.249. The cohesive energy, E_{coh}, of elemental solids is the difference between the total energies of a solid and of isolated atoms. The calculated values for Cd, Zn and Te are −0.76, −1.13, and −2.91 eV per atom, while the respective experimental values are −1.16, −1.35, and −2.19 eV (Ref. 29).

The calculated lattice constants of CdTe and ZnTe are 6.62 and 6.21 Å, while the experiment gives 6.46 and 6.10 Å, respectively.[30] The cohesive energies of CdTe and ZnTe are the differences in total energy between the bulk E_{CdTe} and E_{ZnTe} and isolated atoms. The calculated $E_{\mathrm{coh}}^{\mathrm{CdTe}}$=−4.61 eV and $E_{\mathrm{coh}}^{\mathrm{ZnTe}}$=−4.98 eV per two atoms are reasonably close to the corresponding experimental values of −4.4 and −4.7 eV;[31] the calculated heats of formation are ΔH_f(CdTe)=−0.94 eV and ΔH_f(ZnTe)=−0.95 eV, while the respective measured values are −0.86 and −0.92 eV.[32] The overall agreement with experiment is satisfactory. Finally, LDA and GGA are known to underestimate the band gaps of semiconductors. In our case, the calculated band gaps $E_{\mathrm{gap}}^{\mathrm{GGA}}$ of ZnTe and CdTe are 1.05 and 0.60 eV, respectively, while the corresponding experimental values $E_{\mathrm{gap}}^{\mathrm{exp}}$ are 2.39 and 1.60 eV.

A. Formation energies

The formation energy of a defect A in a charge state Q is defined as[33]

$$E_{\mathrm{form}}[A^Q] = E_{\mathrm{tot}}[A^Q] - E_{\mathrm{tot}}[\mathrm{bulk}] - \sum_i n_i\mu_i + Q(E_F + E_{\mathrm{VBM}}^{\mathrm{bulk}}) + \xi(Q). \quad (1)$$

Here $E_{\mathrm{tot}}[A^Q]$ is the total energy of a supercell containing the defect, E_{tot}[bulk] is the total energy of the ideal supercell, n_i is the number of ith type of (host or impurity) atoms that are transferred from the supercell to the reservoir while forming the defect, n_i=−1 (+1) if an atom is removed (added), and μ_i is the chemical potential of the ith atomic species. The maximum of the valence band (VBM) of the ideal crystal is denoted by $E_{\mathrm{VBM}}^{\mathrm{bulk}}$, and E_F is the Fermi level referenced to the VBM. When dealing with charged defects, a compensating uniform background has been assumed.[34] The top of the valence band in the ideal supercell, $E_{\mathrm{VBM}}^{\mathrm{bulk}}$, and that in the supercell with a (charged) defect, E_{VBM}, differ by the electrostatic potential ΔV,

$$E_{\mathrm{VBM}} = E_{\mathrm{VBM}}^{\mathrm{bulk}} + \Delta V. \quad (2)$$

The procedure that enables one to relate the two values is described in detail in Refs. 33 and 35. In particular, $E_{\mathrm{VBM}}^{\mathrm{bulk}} = E_{\mathrm{tot}}[\mathrm{bulk}, Q=0] - E_{\mathrm{tot}}[\mathrm{bulk}, Q=1]$. The alignment of the electrostatic potential ΔV was obtained following Ref. 33, i.e., using two methods. First, we compare the potential at

two reference points far from the defect in the supercells with and without the defect. Second, we compare the local density of states (LDOS) of atoms far from the defect. In particular, we consider the energies of strongly localized d(Zn), d(Cd), and s(Te) states that give sharp peaks. Both methods give the same alignment to within 0.05 eV. This term has been evaluated for neutral defects and used for charged states. Makov and Payne[36] showed that because of electrostatic interaction between the periodically spaced charged defects, the total energy converges as $1/\epsilon L$ as a function of the supercell size, where L is the linear dimension of the supercell and ϵ is the static dielectric constant. To compensate for this effect, a correction term $\xi(Q)$ is added, which takes into account the electrostatic energy of point charges in the compensating background. This term is given by the Madelung expression divided by dielectric constant of the host. Since the defect-induced charge density is not pointlike, there is a quadrupole contribution to the electrostatic energy. Typically, the quadrupole term decreases the interaction energy by about 30%,[33] which is included.

The detailed value of the defect-defect interaction depends on the change in the total electron density Δn induced by a defect, which is not pointlike. However, in general, Δn is limited to a distance comparable to the distance to the nearest neighbors, i.e., the perturbation is localized.[37] The localization of Δn is stronger than the localization of individual defect states, which may extend over several unit cells. However, the Makov–Payne (M-P) corrections are expected to be larger for interstitials (inducing deep and localized states) than for vacancies (whose levels are close to VBM and more delocalized). In any case, we stress that the used values, $\xi(Q=1)=0.11$ eV for CdTe and 0.13 eV for ZnTe, are the upper limits for vacancies.

Finally, the defect concentration N is related to its formation energy by $N=N_0 \exp(-E_{\text{form}}/k_B T)$, where N_0 is the density of the appropriate lattice sites.

B. Band and gap corrections

The results of the GGA calculations of defect properties are often corrected to account for the underestimation of the gap. In fact, DFT relates the ground-state energy of an arbitrary system, e.g., a crystal with or without native defects, with its electron density calculated using the Kohn–Sham (K-S) equations.[19] The one-electron K-S states are identified with the actual one-electron states. Solution of the K-S equation requires the knowledge of the exchange and correlation potentials, and typically the local-density approximation (LDA) or GGA is assumed. However, the GGA/LDA K-S eigenenergies underestimate the band gaps of insulators, which may be interpreted as a result of the fact that DFT does not describe properly the excited states of a system. More accurate band-gap energies are obtained within the GW approximation,[38] which shows that the errors mainly arise from the underestimation of the energies of conduction states. The underestimation may also occur in the case of deep defect-induced levels in the band gap, which leads to a question about the accuracy of both the energies of the defect-induced levels and of their formation energies obtained within LDA/GGA. An empirical procedure to correct the LDA/GGA gap errors consists in shifting the energies of defect states and then to accordingly modify formation energies. More precisely, after finding the underestimation of the gap relative to the experimental value, $\Delta E_{\text{gap}}=E_{\text{gap}}^{\text{exp}}-E_{\text{gap}}^{\text{GGA}}$, the GGA defect levels $\varepsilon_{\text{defect}}^{\text{GGA}}$ are shifted upward. One may assume the shift to be proportional to the contribution of the conduction states to the defect level. This contribution, in turn, may be assumed to be proportional to the energy of the level relative to the conduction bands; i.e., the corrected defect energy $\varepsilon_{\text{defect}}^{\text{corrected}}$ is rescaled by the correction of the band gap, and is given by $\varepsilon_{\text{defect}}^{\text{corrected}}=\varepsilon_{\text{defect}}^{\text{GGA}}(E_{\text{gap}}^{\text{exp}}/E_{\text{gap}}^{\text{GGA}})$. Thus, the levels close to the top of the valence band are almost nonshifted, while the levels close to the conduction band are shifted by about ΔE_{gap}. Finally, the formation energy of the defect is increased by $\varepsilon_{\text{defect}}^{\text{corrected}}-\varepsilon_{\text{defect}}^{\text{GGA}}$ times the number of electrons that occupy the gap state. This approach is empirical. In particular, considering the energy corrections, energies of shallow effective-mass donors, whose wave functions are built up from the states close to the minimum of the conduction band, are expected to shift by the same amount as the bottom of the conduction band itself. Corrections of the deep levels are less straightforward, since their wave functions are derived from various bands and various points of the Brillouin zone. For example, the wave functions of the interstitials are considered to have a nonbonding character, and thus the contribution of the conduction states should not be dominant. The actual procedure used here to correct the GGA gap error is discussed in detail in Sec. IV.

A better justified scheme improving some of the LDA/GGA deficiencies is the LDA+U approach, which provides a better description of correlation effects important in the case of localized d orbitals. In particular, the LDA energies of d(Zn) are too high; thus the coupling between d(Zn) and the top of the valence band is overestimated, which results in an overestimation of its upward shift. This effect is important in ZnO,[39] where the energy of d(Zn) is close to the VBM, and the LDA energy of the VBM is overestimated by 0.8 eV.[40] On the other hand, the energy of d(Zn) in ZnTe is lower, and the overestimation is 0.2 eV only.[40] A similar overestimation is expected for CdTe, since according to our results both d(Zn) in ZnTe and d(Cd) in CdTe are $\sim$7 eV below the VBM. Finally, even in ZnO, the differences between LDA and LDA+U formation energies are about 0.3 eV,[39] and the LDA gap corrections lead to much larger changes in formation energies. Consequently, we neglected the LDA+U corrections.

C. Chemical potentials

The chemical potential of ith atomic species μ_i is referenced here to the chemical potential of the elemental solid μ_i^{bulk} according to

$$\mu_i = \mu_i^{\text{bulk}} + \Delta\mu_i. \tag{3}$$

The cohesive energy of the elemental solid is obtained by subtracting the energy of the isolated atom from μ_i^{bulk}. Chemical potentials depend on experimental growth conditions, which range from cation-rich to Te-rich. They deter-

mine formation energies because formation of a defect requires exchange of atoms between the host and the reservoirs. For instance, when a substitutional Zn_{Cd} is created, a Zn atom is taken from the reservoir of Zn and embedded into the host substituting Cd, and the Cd atom is removed from the host and put into the reservoir of Cd. Consequently, E_{form} of Zn_{Cd} increases when μ_{Zn} decreases and/or μ_{Cd} increases, as explicitly reflected in Eq. (1).

Chemical potentials are variables subject to firm bounds. For example, μ_{Cd} assumes the maximum value when the growth occurs under Cd-rich conditions, that is,

$$\mu_{Cd} = \mu_{Cd}^{bulk} \quad \text{and} \quad \Delta\mu_{Cd} = 0. \tag{4a}$$

Thermodynamic equilibrium requires that μ_{Cd} cannot be higher than the energy of bulk Cd, μ_{Cd}^{bulk}; otherwise, precipitates of metal Cd in the bulk or at the surface would form. Similarly, Zn- or Te-rich conditions define the upper limits of μ_{Zn} by $\Delta\mu_{Zn}=0$ and $\Delta\mu_{Te}=0$, respectively. On the other hand, the lower bounds of chemical potentials are given by, e.g.,

$$\Delta\mu_{Cd} + \Delta\mu_{Te} = \Delta H_f(\text{CdTe}), \tag{4b}$$

where ΔH_f(CdTe) is the heat of formation of CdTe. Thus, in the case of CdTe under Cd-rich conditions, $\Delta\mu_{Cd}=0$ eV and $\Delta\mu_{Te}=\Delta H_f(\text{CdTe})=-0.94$ eV; and under Te-rich conditions, $\Delta\mu_{Cd}=\Delta H_f(\text{CdTe})=-0.94$ eV and $\Delta\mu_{Te}=0$ eV. Analogous relations hold for ZnTe.

Finally, possible formation of secondary phases between a dopant A and the constituents of a compound BC imposes additional limitations on the chemical potential of A, which in general affect dopant solubilities.[33,35,41] In the case under study, when, e.g., Zn is introduced in CdTe, it should be treated as a dopant. Consequently, besides bounds (4a) and (4b), formation of ZnTe as a secondary phase in CdTe (and CdTe as secondary phase in ZnTe) should be considered. This imposes additional upper bounds on dopants in the considered compounds,

$$\Delta\mu_{Zn} + \Delta\mu_{Te} = \Delta H_f(\text{ZnTe})$$

and for Zn in CdTe and

$$\Delta\mu_{Cd} + \Delta\mu_{Te} = \Delta H_f(\text{CdTe}) \tag{5}$$

for Cd in ZnTe. In particular, in the case of Zn in CdTe under Cd-rich growth conditions, $\Delta\mu_{Cd}=0$ eV, $\Delta\mu_{Te}=\Delta H_f(\text{CdTe})=-0.94$ eV according to Eqs. (4a) and (4b), and $\Delta\mu_{Zn}=\Delta H_f(\text{ZnTe})-\Delta\mu_{Te}=\Delta H_f(\text{ZnTe})-\Delta H_f(\text{CdTe})=-0.01$ eV according to Eq. (5). Thus, the excess chemical potentials of Zn and Cd are practically equal and vanishing. In this particular case, additional constraints (5) have no practical implications because ΔH_f(ZnTe) and ΔH_f(CdTe) are equal to within 0.01 eV. For the same reason, the chemical potentials of Zn and Cd are equal in all the remaining cases. However, it should be stressed that in general, when ΔH_f of the compounds under study are different, constraints (5) strongly affect the results. Similarly, the formation of secondary phases such as $Cd_{0.5}Zn_{0.5}Te$ practically does not affect the chemical potentials of Zn and Cd. This is because the heat of formation of $Cd_{0.5}Zn_{0.5}Te$ is equal to ΔH_f(ZnTe) or ΔH_f(CdTe) to within 0.01 eV. In other words, the mixing enthalpy of CdZnTe alloy is about 10 meV.

The transition energy level of a defect, $\varepsilon(Q/Q')$, is the Fermi energy at which the formation energies of the charge states Q and Q' are equal. These levels are observed in experiments such as deep-level transient spectroscopy, where in the final state the defect relaxes to its equilibrium configuration. In optical experiments, optical transitions are much faster than lattice relaxation to equilibrium. Accordingly, the transition energy between the charge states Q and Q', $\varepsilon^{opt}(Q/Q')$, is obtained when in the final state Q' the atomic configuration is that of the initial state Q. Atomic relaxations of the final state give Franck–Condon shifts. Finally, in principle, free energy should be used in Eq. (1), but in general contributions of vibrational entropy are small and do not affect qualitative conclusions.[35] Summarizing, all factors considered, the errors in the calculated formation energies and energy levels are estimated to about 0.2 and 0.1 eV, respectively. The errors can be larger for very localized defects in high charge states.[35,42]

III. CATION VACANCIES IN CdTe AND ZnTe

Formation of a vacancy implies a formation of four dangling bonds of the four neighbors. In a zinc-blende host, their linear and symmetrized combinations result in a singlet a_1 and a triplet t_2 that is located higher in energy. Their energies relative to the top of the valence band depend on the host. These four orbitals may accommodate up to eight electrons. Because each Te bond is occupied with 6/4 electrons, the levels of a neutral cation vacancy are occupied with $4(6/4)=6$ electrons. Two of them are located on the a_1 singlet and the remaining four on the t_2 triplet. Thus, a neutral cation vacancy in II–VI compounds has two empty states on t_2 and is a double acceptor. The fact that the states induced by both V_{Cd} and V_{Zn} are formed by Te dangling bonds explains the similarities between the two defects that are discussed below. Next, since vacancy states are derived mostly from the valence states, energies of vacancy levels relative to the top of the valence band are determined accurately in spite of substantial band-gap errors typical for GGA. In both CdTe and ZnTe, the a_1 singlet is resonant with the valence band and is located at about 2 eV below the top of the valence bands. The t_2 triplet is at about 0.1 eV above the VBM in both

TABLE I. Energies of the vacancy-induced triplet state t_2, changes in the distances to the first (Δd_1) and second (Δd_2) neighbors, and total energies gains due to relaxation ΔE_{relax} for neutral and charged states of V_{Cd} in CdTe. Δd is defined as the difference between the relaxed and unrelaxed bond lengths relative to the unrelaxed bond. Negative Δd means inward relaxation.

	V_{Cd}^{0}	V_{Cd}^{-}	V_{Cd}^{--}
t_2 (eV)	0.04	0.05	0.08
Δd_1 (%)	−7.96	−7.64	−8.70
Δd_2 (%)	−1.86	−1.85	−2.31
ΔE_{relax} (eV)	0.23	0.30	0.47

TABLE II. Energies of the vacancy-induced triplet state t_2, changes in the distances to the first (Δd_1) and second (Δd_2) neighbors, and total energies gains due to relaxation ΔE_{relax} for neutral and charged states of V_{Cd} in ZnTe. Negative Δd means inward relaxation.

	V_{Zn}^{0}	V_{Zn}^{-}	V_{Zn}^{--}
t_2 (eV)	0.05	0.07	0.10
Δd_1 (%)	−4.87	−4.88	−5.51
Δd_2 (%)	−1.31	−1.47	−1.65
ΔE_{relax} (eV)	0.11	0.23	0.41

crystals. The energies of t_2 are listed in Tables I and II. They depend on the charge of defects. The energy of t_2 increases with the growing number of electrons occupying this state, which stems from the increasing electron-electron repulsion.

Figure 1 presents the calculated formation energies of Cd vacancy V_{Cd} in CdTe as a function of the Fermi energy for both Cd-rich and Te-rich conditions. Only line segments that correspond to the charge state with the lowest energy are shown. Thus, the slope of the line reflects the charge state of the defect at a particular E_F, and the change in the slope corresponds to the change in the charge state and determines the transition energy level. Throughout the available values of E_F, the vacancy can assume one of the three charge states, which range from the neutral one in p-type samples to 2− in n-type samples. As it follows from Fig. 1, the calculated transition energy levels from the neutral to the singly charged state V_{Cd}^{-} is $\varepsilon_{V\text{Cd}}(0/-)=0.1$ eV and to the 2− state V_{Cd}^{--} $\varepsilon_{V\text{Cd}}(-/--)=0.25$ eV. Next, the formation of V_{Cd} is easier in the Te-rich limit than in the Cd-rich limit since the formation energy is lower by 0.95 eV, i.e., by the calculated values of ΔH_f(CdTe). Finally, the very low values of E_{form} for high Fermi energies indicate that cation vacancies act as compensating acceptors, as it will be discussed in more details below. The obtained results agree to within 0.1 eV with those of Ref. 17.

The formation energies of the V_{Zn} in ZnTe are shown in Fig. 2. The transition levels $\varepsilon_{V\text{Zn}}(0/-)$ and $\varepsilon_{V\text{Zn}}(-/--)$ are 0.06 and 0.36 eV, respectively. Comparing the results for CdTe and ZnTe, one may see that for given growth conditions (i.e., cation-rich or Te-rich), the formation energy of V_{Zn}^{0} in ZnTe is lower than that of V_{Cd}^{0} in CdTe by 0.28 eV. According to Eq. (1), this result may be due to (a) the lower value of energy necessary to extract a Zn atom from the crystal, given by $E_{\text{tot}}[V_{\text{Zn}}]-E_{\text{tot}}[\text{ZnTe}]$, or to (b) the lower cohesive energy $\mu_{\text{Zn}}^{\text{solid}}$ compared to $\mu_{\text{Cd}}^{\text{solid}}$. The first contribution favors the formation of V_{Cd} in CdTe. This stems from the fact that ZnTe is less ionic than CdTe, and, as a rule, more covalent compounds are characterized by stronger bonds. However, this factor is overcompensated by the fact that the cohesive energy of solid Zn, −1.13 eV, is higher than that of solid Cd, −0.76 eV. Thus, ultimately, this is the higher stability of solid Zn that favors the formation of V_{Zn} over V_{Cd}.

A comparison of the results from Tables I and II shows that the relaxation of atoms neighboring the vacancy depends on its charge state, and the relaxation effects are stronger in CdTe than in ZnTe. The nearest-neighbor Te atoms and 12 second-neighbor cations surrounding a vacancy relax sym-

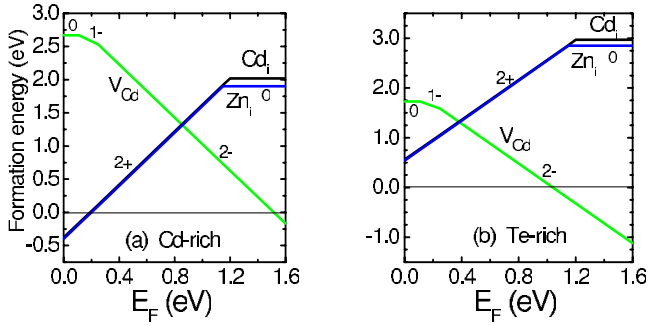

FIG. 1. (Color online) Calculated formation energies of V_{Cd}, Cd_i, and Zn_i in CdTe as a function of the Fermi energy in the (a) Cd-rich and (b) Te-rich limits. The transition energy levels correspond to the values of E_F at which the slope changes.

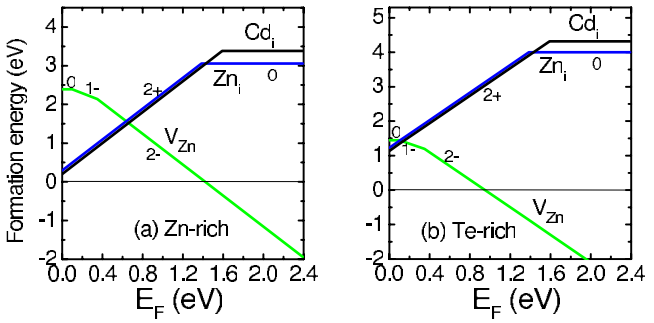

FIG. 2. (Color online) Calculated formation energies of V_{Zn}, Cd_i, and Zn_i in ZnTe as a function of the Fermi energy in the (a) Zn-rich and (b) Te-rich limits.

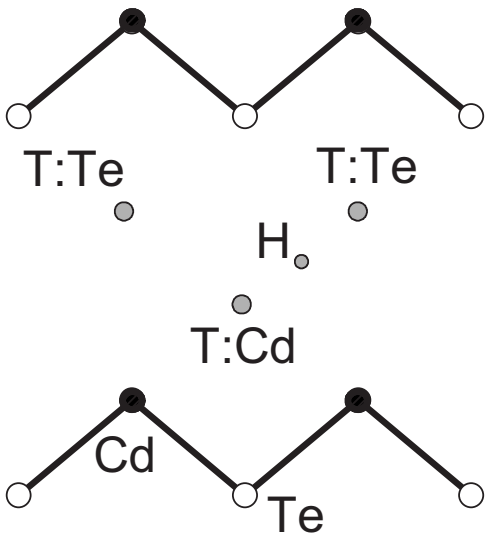

FIG. 3. Locations of the two tetrahedral (T) and of the "hexagonal" (H) interstitial sites in CdTe in the (110) plane. Cd and Te atoms are represented by solid and open circles, respectively. The x axis is in the [110] direction, and the y axis in the [001] direction. Each tetrahedral site is surrounded by four atoms of the same type, two of which are out of the plane of the figure and are not shown.

TABLE III. Energies of the singlet state a_1, changes in the distances to the first Δd_1 and the second Δd_2 neighbors, and relaxation energies ΔE_{relax} for neutral and charged states of Cd_i in CdTe.

	Cd_i^0		Cd_i^+		Cd_i^{++}	
	T:Cd	T:Te	T:Cd	T:Te	T:Cd	T:Te
a_1 (eV)	0.75	1.10	0.80	1.10	0.90	1.10
Δd_1 (%)	3.72	6.90	6.37	2.76	8.31	1.01
Δd_2 (%)	2.58	0.19	0.29	3.22	−1.64	4.40
ΔE_{relax} (eV)	0.26	0.45	0.31	0.40	0.52	0.60

metrically toward the center. The contraction of the distances and relaxation energy are the highest for doubly charged centers (Tables I and II), when the triplet is fully occupied with six electrons. In the case of V_{Zn}, both the changes in the bond lengths and relaxation energy are smaller than in the case of V_{Cd} since the radius of a Zn atom is smaller than that of Cd and the stiffness of ZnTe is greater (the calculated bulk modulus of ZnTe, 43 GPa, is larger than that of CdTe, 36 GPa).

In the case of neutral and singly charged vacancies, a partial occupation of the t_2 level can lead to the Jahn-Teller distortion. However, the obtained results show that the T_d symmetry of the cation vacancies in both CdTe and ZnTe is maintained. Stability has been verified by imposing appropriate atomic distortions with either C_{3v} or D_{2d} symmetry. For the trigonal distortion, a Te atom along the [111] direction is displaced away from the center, while the other Te atoms are moved toward the center. Tetragonal distortion was imposed by moving along the [110] direction two Te atoms at (1,1,1) and (−1,−1,1) sites toward each other, and simultaneously moving closer Te atoms at (1,−1,−1) and (−1,1,−1) sites along the $[\bar{1}10]$ direction. In both cases, the T_d symmetry is found to be more stable than the distorted one. The same result was obtained in Ref. 15. However, the relatively small supercell used here may be not sufficient to assess the exact geometry of an isolated vacancy; see Ref. 43.

The calculated optical levels for CdTe are $\varepsilon_{V\text{Cd}}^{\text{opt}}(0/-)=0.16$ eV, $\varepsilon_{V\text{Cd}}^{\text{opt}}(0/--)=0.16$ eV, and $\varepsilon_{V\text{Cd}}^{\text{opt}}(-/--)=0.17$ eV. The corresponding Franck–Condon shifts are 0.002, 0.031, and 0.017 eV. For ZnTe we find $\varepsilon_{V\text{Zn}}^{\text{opt}}(0/-)=0.06$ eV, $\varepsilon_{V\text{Zn}}^{\text{opt}}(0/--)=0.18$ eV, and $\varepsilon_{V\text{Zn}}^{\text{opt}}(-/--)=0.34$ eV with the Franck–Condon shifts of 0.005, 0.063, and 0.016 eV. Thus, optical processes entail more relaxation in ZnTe, in spite of the fact that Zn vacancy induces less surrounding relaxation than V_{Cd} in CdTe.

IV. CATION INTERSTITIALS IN CdTe AND ZnTe

In the zinc-blende structure, there are two nonequivalent interstitial sites with the tetrahedral symmetry, the first of which is surrounded by four anions, T:anion, and the other by four cations, T:cation. They are shown in Fig. 3. In an ideal crystal, the distance from these sites to the nearest neighbors is equal to the bond length of the host. The location in the middle between T:cation and T:anion is denoted as H. The results obtained for both Cd_i and Zn_i in CdTe are given in Tables III and IV and shown in Fig. 1, while those for ZnTe are given in Tables V and VI and shown in Fig. 2.

According to the obtained results, interstitials at both sites induce a singlet state a_1 located in the upper half of the band gap, about 1.5 eV above the top of the valence band. This follows from the fact that an atom located at an interstitial site is surrounded by host atoms that have formed bonds with their four (host) neighbors. Consequently, the electrons of an interstitial do not form bonds with its neighbors, and the induced gap states are predominantly of nonbonding character. The a_1 level of the neutral interstitial is occupied by the number of electrons that is equal to the valence of the interstitial atom, i.e., by two electrons of cation interstitials in II–VI compounds. The Kohn–Sham energies of a_1 corrected for the GGA underestimation of the gap are given in Tables III and IV.

A. Zn and Cd interstitials in CdTe

The calculated formation energies of Cd_i and Zn_i in CdTe as a function of the Fermi energy in Cd-rich conditions for minimum formation energy locations are presented in Fig. 1. The difference in E_{form} between the Cd-rich and Te-rich limits is the heat of formation of a given compound, in accord with Eqs. (4a) and (4b).

As it was mentioned above, both interstitials induce levels in the upper part of the gap, which may lead to errors in

TABLE IV. Energies of the singlet state a_1, changes in the distances to the first Δd_1 and the second Δd_2 neighbors, and relaxation energies ΔE_{relax} for Zn_i in CdTe. Negative Δd means inward relaxation.

	Zn_i^0		Zn_i^+		Zn_i^{++}	
	T:Cd	T:Te	T:Cd	T:Te	T:Cd	T:Te
a_1 (eV)	0.85	1.20	0.85	1.20	0.85	1.20
Δd_1 (%)	1.25	2.53	3.55	−1.35	6.86	−3.00
Δd_2 (%)	2.06	1.50	0.21	3.50	−2.45	4.38
ΔE_{relax} (eV)	0.09	0.35	0.37	0.50	0.55	0.85

TABLE V. Energies of the singlet state a_1, changes in the distances to the first Δd_1 and the second Δd_2 neighbors, and relaxation energies ΔE_{relax} for neutral and charged states of Cd_i in ZnTe.

	Cd_i^0		Cd_i^+		Cd_i^{++}	
	T:Zn	T:Te	T: Zn	T:Te	T:Zn	T:Te
a_1 (eV)	1.55	1.85	1.60	1.90	1.60	1.95
Δd_1 (%)	3.16	8.73	5.23	6.55	7.06	5.04
Δd_2 (%)	4.00	0.68	2.24	2.19	0.86	3.22
ΔE_{relax} (eV)	0.41	0.89	0.40	0.83	0.53	0.95

formation energies calculated within GGA. A scheme to estimate and correct these errors, indicated in Sec. II B, is now applied to both interstitials, and the results are shown in Figs. 4 and 5. Figure 4 shows E_{form} of Cd_i in CdTe for both interstitial sites obtained using (a) GGA, (b) GGA and the M-P corrections, and (c) including both the M-P corrections and shifting the interstitial energies by the underestimation of the band gap $\Delta E_{\text{gap}}=E_{\text{gap}}^{\text{exp}}-E_{\text{gap}}^{\text{GGA}}$. From Fig. 4 it follows that the M-P corrections and the gap corrections act in opposite ways. The M-P corrections decrease E_{form} of the charged defects, and thus increase the difference between the transition levels $\varepsilon(0/+)$ and $\varepsilon(+/2+)$. In contrast, the gap corrections increase E_{form} of interstitials in the neutral and 1+ charge states, which favors the negative-U situation. Cd_i is a negative-U defect in the GGA, a positive-U defect after the M-P corrections, and again negative-U with the gap corrections included. The final results (with both M-P and band-gap corrections) for both interstitials in CdTe and ZnTe are shown in Figs. 1 and 2, respectively.

In agreement with the fact that cation interstitials are donors, their charge state depends on the Fermi energy and is neutral in n-type samples and 2+ in p-type samples. As it follows from Figs. 1 and 2, formation energies of neutral interstitials are relatively large, and their equilibrium concentrations are lower than 10^6 cm^{-3} [computed by supposing $T=600$ K, i.e., the temperature of molecular-beam-epitaxy (MBE) growth of CdZnTe samples]. Thus, they play a negligible role in n-type samples. In contrast, in p-type samples Cd_i^{++} have low formation energies and they are the dominant compensating donors, as it is discussed in Sec. VI.

A comparison of the results in Figs. 1 and 2 shows that under Cd-rich conditions, the expected concentrations of Zn_i and Cd_i at the T:Te sites are high and very close. Relative energies of interstitials at the T:Te and T:Cd sites are discussed in detail in Sec. V, devoted to the interstitial diffusion.

Formation energies are affected by atomic relaxations. As it follows from Tables III and VI, the sign and magnitude of lattice relaxation effects depend on the charge state and on the interstitial site. In particular, neutral interstitials induce fully symmetric breathing-mode outward displacements of neighbors. For example, in the case of Cd_i at the T:Cd site, the outward relaxation of the first neighbors, Δd_1, increases from 3.7% for the neutral to 8.3% for the doubly charged state, while simultaneously the distance to the six second neighbors, Δd_2, decreases. These tendencies can be explained in terms of simple electrostatic considerations based on the fact that cations are positively charged and anions are negatively charged: an interstitial located at the T:cation site repels the cation neighbors more strongly when it is more positively charged. The opposite effect is expected and found for the second neighbors, which are Te anions. For Cd_i at the T:Te site, the increased Coulomb attraction explains why the outward relaxation of anions, given by Δd_1, is reduced from 6.9% for the neutral state to 1% for the 2+ state. Finally, in agreement with the nonbonding character of the defect-induced a_1 states, their energies are practically not affected by the relaxation effects.

It is relevant to compare formation energies of Cd_i in CdTe with those calculated in Ref. 17, using the linearized augmented plane-wave (LAPW) method and neglecting the M-P corrections. LAPW gives an almost correct gap of CdTe, and therefore the gap corrections are not necessary. For the neutral Cd_i the results in Figs. 4(a) and 4(b), 1.6 and 2.4 eV, respectively, bracket the value 2.0 eV of Ref. 17. Moreover, in the spirit of arguments presented in Sec. II B, the midgap interstitial levels should be corrected by one-half of the band-gap error. Applying this correction leads to a very good agreement with both E_{form} and the transition level energies of Cd_i in CdTe. However, the accuracy is too low to unambiguously assess the negative-U character of the defect. A more detailed comparison is not possible, since in Ref. 17 E_{coh} of elemental Cd and Te are not given.

B. Zn and Cd interstitials in ZnTe

We now turn to Cd and Zn interstitials in ZnTe. The results are shown in Figs. 1 and 2 and in Tables V and VI. In general, the calculated properties of both interstitials are similar to those in CdTe. In particular, both interstitials are donors with the singlet a_1 state located in the upper half of the band gap.

TABLE VI. Energies of the singlet state a_1, changes in the distances to the first (Δd_1) and the second Δd_2 neighbors, and relaxation energies ΔE_{relax} for Zn_i in ZnTe.

	Zn_i^0		Zn_i^+		Zn_i^{++}	
	T: Zn	T:Te	T:Zn	T:Te	T:Zn	T:Te
a_1 (eV)	1.45	1.90	1.45	1.90	1.35	1.90
Δd_1 (%)	0.44	4.64	3.31	2.47	5.19	0.87
Δd_2 (%)	2.96	1.17	1.03	2.36	−0.47	3.40
ΔE_{relax} (eV)	0.15	0.26	0.14	0.32	0.28	0.56

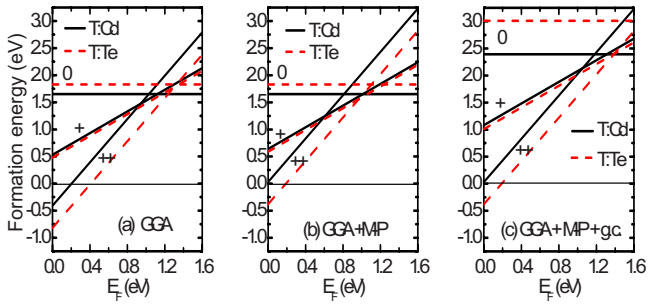

FIG. 4. (Color online) Calculated formation energies of Cd_i in CdTe as a function of the Fermi energy at the Cd-rich limit for both the T:Cd and T:Te sites. (a) Bare GGA results and those after including (b) the M-P corrections and (c) both the M-P and the gap corrections. See text for details.

Zn_i in ZnTe was considered in Ref. 44. The results given in Fig. 2, obtained using the M-P expression and corrected for the half of the underestimation of the GGA band gap, agree with those of Ref. 44 to within 0.2 eV. A more detailed comparison is not possible, since in Ref. 44 the correction of the band gap refers to its value at the mean value point rather then to the gap calculated at Γ.

Analysis of the obtained results allows drawing several general conclusions regarding the properties of interstitials as follows:

(1) Energy levels (Tables III–VI) as well as transition energies (Figs. 1 and 2) of Zn_i are lower that those of Cd_i by about 0.3 eV. This holds for both T:Te and T:cation sites and for both CdTe and ZnTe hosts. The effect follows from the fact that the interstitial-induced a_1 level has a nonbonding character, and thus it mainly reflects the energy of the relevant orbital of an isolated atom. In fact, the energy of an s orbital of isolated Zn, −5.96 eV, is about 0.3 eV lower than that of Cd, −5.64 eV (both values are obtained for the employed pseudopotentials).

(2) A comparison of Figs. 1 and 2 with the corresponding Tables III–VI shows that the transition energies relative to the VBM of both interstitials at both sites in ZnTe are higher than those in CdTe. This result agrees with the fact that the top of the valence band of ZnTe is lower than that in CdTe, as the experimental valence-band discontinuity in a ZnTe/CdTe heterojunction is 0.10 eV.[45] Thus, because of their nonbonding character, interstitial states may be regarded as "absolute reference levels."

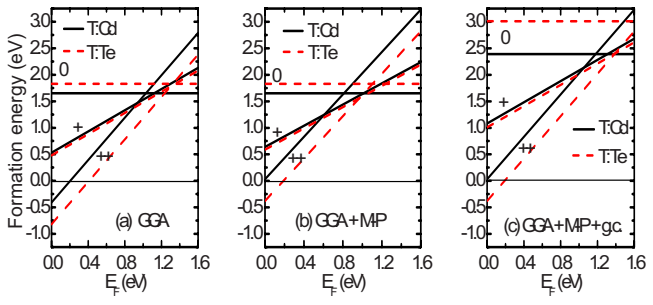

FIG. 5. (Color online) Calculated formation energies of Zn_i in CdTe as a function of the Fermi energy at the Cd-rich limit for both the T:Cd and T:Te sites. (a) Bare GGA results and those after including (b) the M-P corrections and (c) both the M-P and the gap corrections. See text for details.

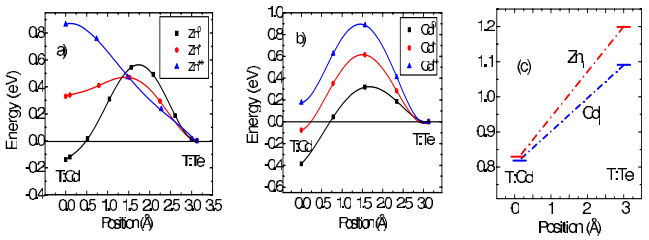

FIG. 6. (Color online) The total energy of (a) Zn_i and (b) Cd_i in CdTe as a function of the location along the diffusion path for three charge states. The zero of energy is assumed at the T:Te site. (c) shows the energy of the a_1 level at both tetrahedral sites for Zn_i and Cd_i. The lines are guide for the eyes.

(3) Formation energies of Zn_i are in general lower than those of Cd_i. The energy difference is about 0.35 eV in the neutral state; see Figs. 1 and 2. The effect follows from the smaller atomic radius of Zn. In fact, it was mentioned in the beginning of this section that both interstitials induce nonnegligible outward displacements of neighbors, and thus generate excess elastic energy of local strains. On the other hand, for low Fermi energies, i.e., for the 2+ charge state, the stable sites of both defects are T:Te, and the formation energies of Zn_i and Cd_i are almost equal according to Figs. 1 and 2. In this case, the strain is lower for Cd_i, for which $\Delta d_1 = 1\%$, than for Zn_i, for which $\Delta d_1 = -3\%$.

(4) Strain effects also explain the fact that formation energies of interstitials in ZnTe are higher than in CdTe by about 0.7–0.8 eV. This effect follows from the smaller lattice constant and higher stiffness of ZnTe, and thus higher strain energies generated by interstitials.

V. DIFFUSION OF Cd AND Zn INTERSTITIALS IN CdTe AND ZnTe

Diffusion of self-interstitials occurs along paths that contain the interstitial tetrahedral sites, i.e., along the T:Te-T:Cd-T:Te path shown in Fig. 3. Changes in the total energy of both Zn and Cd interstitials as a function of their location along the diffusion path in CdTe and ZnTe are presented in Figs. 6 and 7, respectively. Both neutral and positively charged defects were considered. The results strongly depend on the charge state.

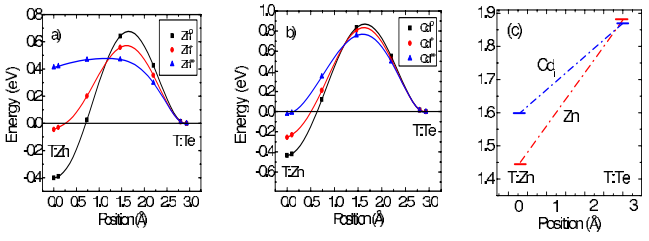

FIG. 7. (Color online) The total energy of (a) Zn_i and (b) Cd_i in ZnTe as a function of the location along the diffusion path for three charge states. The zero of energy is assumed at the T:Te site. (c) shows the energy of the a_1 level at both tetrahedral sites for Zn_i and Cd_i. The lines are guide for the eyes.

We begin with neutral defects. As it was discussed in Sec. IV, in all cases under study the stable location of interstitials is T:cation, while the T:Te sites are metastable. More precisely, the total energy of both Cd_i and Zn_i at T:Cd in CdTe is lower than at the T:Te site by 0.4 and 0.15 eV, respectively; see Fig. 6. In ZnTe, the stability at T:Zn is more pronounced, since the energy of both interstitials at T:Zn is lower by 0.4 eV; see Fig. 7. The maximum of the energy barrier separating the two sites is close to the H site shown in Fig. 3. Diffusion can occur by thermally activated jumps between the two types of sites, and is determined by the larger barrier. In the case of CdTe, the diffusion barriers of both Zn_i^0 and Cd_i^0 are close, about 0.7 eV in CdTe (Fig. 6) and somewhat higher, 1.1 eV, in ZnTe (Fig. 7). The barriers for the reverse jumps from the metastable T:Te to the stable T:cation sites are higher in ZnTe and amount to 0.7 eV. In CdTe, these barriers are lower, 0.5 and 0.3 eV for Zn_i^0 and Cd_i^0, respectively.

The energetics and diffusion of a doubly charged Zn_i^{++} in CdTe is qualitatively different than that of the neutral one; see Fig. 6(a). In fact, the only stable site is T:Te, while the T:Cd site, which is the ground-state configuration of the neutral Zn_i^0, corresponds to the maximum of the energy barrier. Consequently, the diffusion occurs by long and curvilinear jumps between two adjacent T:Te sites with the energy barrier of 0.85 eV. From Fig. 7 it follows that a similar situation takes place also for Zn_i^{++} in ZnTe, where the energy barrier is close to 0.4 eV, and the T:Zn site is a center of a large energy plateau between adjacent T:Te sites. Finally, interstitial Cd_i^{++} in both CdTe and ZnTe diffuses with a barrier of 0.85 eV between T:Cd and T:Te sites. In ZnTe, its energies are identical within our accuracy. In CdTe, the T:Cd site is less stable by about 0.2 eV than the T:Te site.

Analysis of these results shows that the energetics of interstitials, i.e., the dependence of total energy on the location in the unit cell and on the charge state, is determined by two factors. The first one is the dependence of energy of the defect-induced a_1 level on the defect location, shown in Fig. 6(c) for CdTe and in Fig. 7(c) for ZnTe. The second factor is the ionicity of the host. Both factors will now be discussed.

Relative energies of interstitials at T:cation and T:Te sites are mainly determined by energies of the a_1 levels. In particular, in the case of Zn_i in CdTe, the a_1 level decreases by 0.4 eV from 1.2 to 0.8 eV when the interstitial moves from T:Te to T:Cd; see Fig. 6(c). This fact does not affect the energy of Zn_i^{++}, since for this charge state the a_1 level is empty. In contrast, in the case of the neutral Zn_i this level is occupied with two electrons, and the shift of Zn_i from T:Te to T:Cd induces an energy gain of 2×0.4 eV$=0.8$ eV that stabilizes Zn_i at the T:Cd site, which correlates well with the total energy gain of 1 eV. Similarly, in the case of Cd_i at T:Cd in CdTe, the total energy of Cd_i^0 is 0.6 eV lower than that of Cd_i^{2+} [Fig. 6(b)], which is fully accounted for by the change in the energy of the doubly occupied a_1 by 0.3 eV [Fig. 6(c)]. Comparison of Figs. 7(a) and 7(b) with Fig. 7(c) shows that the same explanation is also valid for interstitials in ZnTe. Moreover, results found for singly charged interstitials are intermediate between these for neutral and doubly charged defects.

Turning to the effects of the ionicity of the host we observe that in the case of interstitials in the 2+ state, the energy difference between the T:Te and T:cation is higher in the more ionic CdTe due to Coulomb interactions. This is in line with charge dependence of the interstitial-host bond lengths discussed in Sec. IV. These results are also consistent with those of Ref. 44 studying ZnO, ZnS, ZnSe, and ZnTe, in which the ionicities differ due to the different anions (and not cations, as in our case). This indicates that the role of ionicity has a universal character. Moreover, the ionicity of the host may play a role even in the case of neutral interstitials. From Figs. 6 and 7 it follows that the energy of a neutral interstitial is lower in T:cation than in T:Te, and this difference is higher in less ionic ZnTe. This trend is also present in the series of compounds studied in Ref. 44.

Interestingly, Figs. 6 and 7 suggest that diffusion of neutral Zn_i in both CdTe and ZnTe can be enhanced by injection of holes or illumination of the sample. The mechanism is similar to the Bourgoin–Corbett mechanism of athermal recombination-enhanced diffusion provoked by successive capture/emission of electrons by a defect.[46] In fact, the T:cation site is stable for a neutral Zn_i, but is an energy maximum for Zn_i^{++}. Consequently, after a capture of two holes, Zn_i^{++} relaxes with no energy barrier to the T:Te site. Here, either the interstitial persists in the 2+ state and migrates with the barrier of 0.4 eV in ZnTe (0.85 eV in CdTe), or it captures two electrons and returns to the stable T:cation site with the barrier of 0.6 eV (ZnTe) or 0.5 eV (CdTe). In both cases (except Zn_i^{++} in CdTe), the effective diffusion barrier is *reduced* relative to that of the neutral interstitial.

TABLE VII. Calculated diffusion barriers (in eV) for different configurations and charged states of Zn_i in ZnTe.

Starting point	Charge state	This work (NEB)	Ref. 44
T:Te	0	0.64	0.24
T:Te	+	0.56	0.27
T:Te	2+	0.44	0.45
T:Zn	0	1.04	0.80
T:Zn	+	0.60	0.47
T:Zn	2+	0.03	0.15

Table VII summarizes the obtained diffusion barriers with those of Ref. 44 that were calculated using a "direct" approach, i.e., by fixing the position of an interstitial at a number of sites between T:cation and T:Te. Comparison of the two methods indicates that the two methods give qualitatively similar results, but in general the NEB barriers are higher, which is surprising since in principle NEB allows to find the lowest barriers.

Summarizing, the most important result of this section is that the diffusion barriers are rather small, 0.45–1.05 eV, what implies the possible mobility of interstitials even at room temperature. Next, relative energies of an interstitial at the two tetrahedral sites as well as their energy dependencies on the charge state are almost completely determined by the energy of the a_1 state, its occupation by electrons, and its dependence on the location of the interstitial.

VI. COMPENSATION OF DOPING BY CATION VACANCIES AND CATION INTERSTITIALS

As if follows from Figs. 1 and 2 and Eq. (1), formation energies of defects depend on the Fermi level and growth conditions embedded in chemical potentials of the relevant atomic species. In particular, E_{form} of cation vacancies in both CdTe and ZnTe decreases with the increasing Fermi energy and assumes very low values when E_F approaches the bottom of the conduction band. Therefore, because of their acceptor character, V_{Cd} and V_{Zn} are the dominant native acceptors that compensate p-type doping, and they set up an intrinsic limit on the possible n-type doping of both CdTe and ZnTe.[17] This tendency is weaker when the growth occurs under cation-rich conditions, when formation energies of both V_{Cd} and V_{Zn} are higher. Finally, formation energies are lower in ZnTe than in CdTe, which explains bigger difficulties of obtaining n-ZnTe than n-CdTe.[47]

Cd and Zn interstitials are the dominant intrinsic donors that compensate p doping, which follows from their very low formation energies for low values of the Fermi energy. To minimize compensation, growth should be carried out under Te-rich conditions, when formation of interstitials is more difficult than under cation-rich conditions. Because of higher formation energies of cation interstitials in ZnTe than in CdTe, less limits for p-type doping exist in the latter compound, again in agreement with experiment.[47]

VII. GENERATION AND STABILITY OF VACANCY-INTERSTITIAL FRENKEL PAIRS

A nearest-neighbor vacancy-interstitial Frenkel pair is created by displacing an atom from the lattice site along the [111] direction. In the final configuration the interstitial is displaced by about 6 Å from its site. In this section, we analyze this process for both cation and anion sublattices, beginning with the former case. In most cases FPs are metastable, since there are finite-energy barriers for the return of the interstitial atom to the substitutional site, i.e., for the defect recombination.

A. Cation sublattice

In this case, a cation shifted from equilibrium is close to the T:Te site; see Fig. 3. Changes in the total energy corresponding to the formation of FPs in CdTe and ZnTe are shown in Figs. 8 and 9. The calculated barriers are given in Table VIII. The results show that formation of FPs is very similar in CdTe and ZnTe. The most characteristic feature is the strong dependence of energy barriers and stability of FPs on the complex's charge state that we now discuss.

1. q=0 case

In intrinsic samples, the energy barriers are 2.5–3.0 eV. The final configuration of the nearest-neighbor *V-I* pair is relatively stable, since the calculated energy barriers for recombination are about 0.5 eV.

2. q=2− case

In n-type samples, after capturing two electrons the FP is in the 2− charge state. Figure 9 summarizes the results for

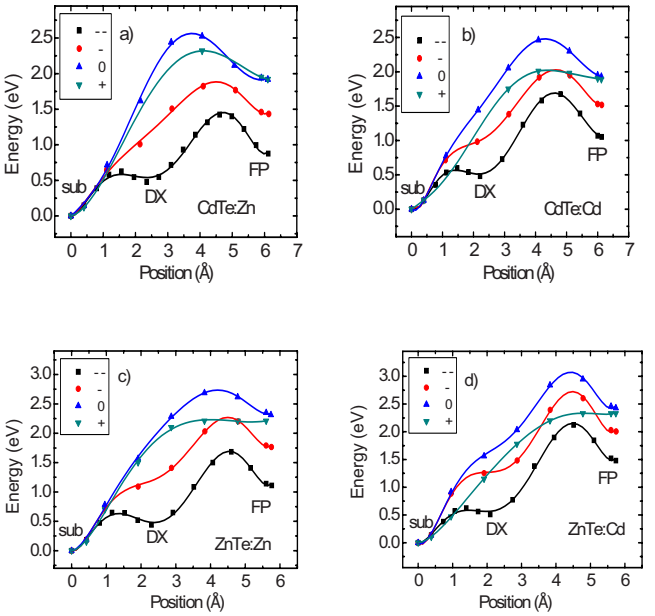

FIG. 8. (Color online) Total energy change corresponding to a creation of (a) V_{Cd}+Zn_i and (b) V_{Cd}+Cd_i Frenkel pairs in CdTe, and (c) V_{Zn}+Zn_i and (d) V_{Zn}+Cd_i FPs in ZnTe as a function of the distance from the substitutional site (sub) for four charge states.

the four considered FPs. The $q=2-$ case is qualitatively different from the remaining charge states because the formation of the FP is preceded by stabilization of a configuration of the *DX* character, in which the interstitial-vacancy separation is 2.3–2.5 Å. This configuration corresponds to the local energy minima in Figs. 8 and 9. The barriers to form the *DX* centers are relatively low, 0.60–0.65 eV (see Table VIII), and their energies are higher than the ground state by about 0.5 eV. Although barriers for recombination are low, about 0.2 eV, metastability is clearly seen. The calculated metastability of V_{Cd}+Cd_i pairs in CdTe in the *DX* configuration confirms the results of Lany *et al.*[48] Since in Ref. 48 the values of energies and barriers are not given, a detailed comparison is not possible.

Formation of FPs results from larger displacements of about 6 Å. The process of formation may occur either in two steps, i.e., with the *DX* configuration mediating the transition

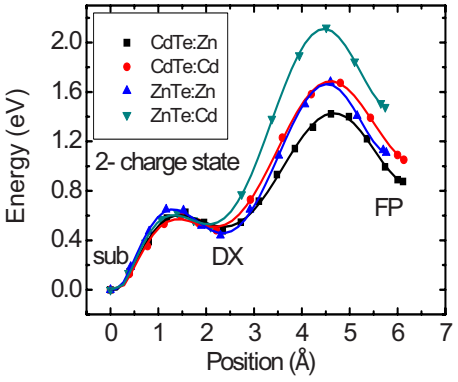

FIG. 9. (Color online) Total energy change corresponding to a creation of Frenkel pairs in the 2− charge state.

TABLE VIII. Calculated diffusion barriers (in eV) for different configurations and charge states of Frenkel pairs in CdTe and ZnTe.

		Barriers			
Path	Charge state	CdTe:Cd	CdTe:Zn	ZnTe:Cd	ZnTe:Zn
Sub-FP	0	2.45	2.55	2.95	2.70
FP-sub	0	0.55	0.60	0.50	0.40
Sub-FP	−	1.95	1.80	2.60	2.20
FP-sub	−	0.45	0.40	0.60	0.45
Sub-*DX*	2−	0.60	0.60	0.60	0.65
DX-FP	2−	1.20	0.95	1.60	1.25
FP-*DX*	2−	0.60	0.55	0.65	0.60
DX-sub	2−	0.10	0.15	0.10	0.20
Sub-FP	+	2.00	2.30	2.35	2.20
FP-sub	+	0.10	0.45	0.00	0.00

to the final FP geometry, or in one large hop. The former possibility involves overcoming two consecutive barriers that are relatively low, while the latter case involves larger barriers of about 1.5 eV. A detailed evaluation of the relative efficiencies of both paths is outside the scope of the paper. However, Fig. 8 shows that in both cases the energy barriers are substantially reduced with respect to the $q=0$ values. The barriers for defect recombination for all cases are about 0.5 eV, which implies a stability of FPs.

The obtained results, i.e., the metastability of the complex and the increased efficiency of FP generation in the presence of excess electrons, are similar to the features characterizing both *DX* centers and the *EL*2 defect in GaAs.[49,17] This similarity stems from the common physical origin: a large displacement of an impurity, or of a host atom, from the substitutional site induces a deep level in the gap, which energy decreases with the increasing displacement. This in turn induces a decrease in the total energy and the stabilization of the *DX* configuration when the gap state is occupied with two electrons in the 2− charge state. In the real space, the wave function of the deep state is localized on the broken bond,[49] and thus the occupation of this state by electrons corresponds to passivation of the broken bond created by the formation of the complex. However, we note that *DX* centers are less stable than FPs: while the *DX* configuration is metastable only in the 2− charge state (and thus is unstable after optical emission of an electron, or its recombination with free holes), FPs are metastable in the $q=1-,0$, or even the $q=1+$ charge states [see case (iv) below], and the relevant barriers are higher.

3. $q=1-$ case

In the intermediate case of the 1− charge state (i.e., when one additional electron is captured by the complex), barriers are also intermediate between those for $q=0$ and $q=2-$, i.e., about 2 eV. The total energy curves display a nonlinear dependence on the *V-I* separation, indicating the tendency to stabilize the *DX* configuration in the 2− state.

4. $q=1+$ case

The energy required to form a FP in a *p*-type sample is very similar to that for the $q=0$ case. However, the barriers for recombination in CdTe are reduced for V_{Cd}+Cd_i, and they even vanish in ZnTe. This means that in *p*-type samples the nearest-neighbor FPs have a lowered stability in CdTe and are not stable in ZnTe.

Finally, as it follows from Figs. 8 and 9, the properties of the V_{Cd}+Zn_i FP in CdTe differ from those of the remaining cases. First, the generation energy of the pair in the 2− state, 1.4 eV, is the smallest. In other cases it amounts to about 1.8 eV, implying a less efficient generation. (Since the generation probability depends exponentially on the barrier height, the difference of 0.2 eV in the barrier leads to a difference of 3 orders of magnitude in generation efficiency.) Second, this is the only FP expected to be stable for charge states from 1+ to 3−. These results are significant in the context of the experimental data discussed in Sec. VIII.

Formation of *V-I* pairs on the cation sublattice in GaAs, CdTe, and NaCl has been considered by Wei *et al.*,[14] who used unit cells containing from 4 to 16 atoms. These cells are too small for a correct description of the energetics of FPs, which are relatively extended defects. In fact, these cells have lateral dimensions close to the equilibrium distance between vacancy and interstitial, ~6 Å. One may note that only their[14] calculated energy increase of ~1.75 eV for displacements of ~2.25 Å of neutral Cd or Zn from ideal sites in CdTe is similar to the results of Fig. 8.

B. Anion sublattice

We now turn to formation of a V_{Te}-Te_i pair on the anion sublattice. The corresponding changes in total energy are shown in Fig. 10. For both the negative and the neutral charge states, the barrier exceeds 6 eV and decreases to 4.75 eV for the 1+ charge state. These values are prohibitively large, and the generation of FPs on the anion sublattice may be neglected. The high energy used to generate a V_{Te}-Te_i pair is consistent with the calculated high formation energies under anion-rich conditions and for $E_F=0$ of V_{Te} (3.40 eV), and those of Te_i at both T:Cd (3.50 eV) and T:Te (3.65 eV) sites.

C. Formation energies and binding energies of Frenkel pairs

Formation energy of a FP is given by Eq. (1) and can be expressed as

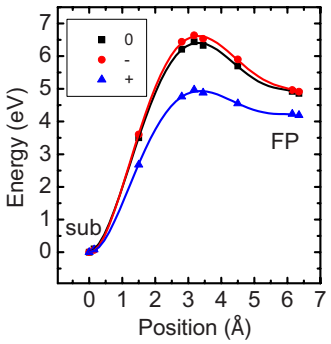

FIG. 10. (Color online) Total energy change corresponding to a creation of V_{Te}-Te_i Frenkel pair in CdTe as a function of the distance from the substitutional site (sub) for three charge states.

$$E_{\mathrm{form}}(V+I) = E_{\mathrm{form}}(V^0) + E_{\mathrm{form}}(I^0) + E^{\mathrm{int}}(V+I) + E^{\mathrm{ord}}(V+I). \tag{6}$$

Here, $E_{\mathrm{form}}(V^0)+E_{\mathrm{form}}(I^0)$ is the sum of the formation energies of a neutral and an isolated vacancy and an interstitial. $E^{\mathrm{int}}(V+I)$ is the interaction energy when V and I are next to each other and form a FP. Finally, in the supercell method, creation of a defect (or of a defect pair) in the unit cell corresponds to formation of an infinite and ordered array of defects that may interact. In the case under study, V-I pairs are electric dipoles that interact by Coulomb forces. The corresponding interaction energy is denoted by $E^{\mathrm{ord}}(V+I)$. In a simple model assuming that the V-I pairs are localized [111]-oriented dipoles, $E^{\mathrm{ord}}(V+I)$ vanishes due to the fact that the supercell is simple cubic. The obtained results are given in Table IX. The dependence on the chemical potentials is negligible because the calculated heat of formation for CdTe and ZnTe are the same to within 0.01 eV; see the discussion in Sec. II B.

There are three contributions to the interaction energy E^{int} of a neutral V-I pair, as follows:

(i) The charge transfer of two electrons from the donor (interstitial) to the acceptor (vacancy). After the charge transfer both the vacancy and the interstitial become charged, and a V-I donor-acceptor pair generates a dipolelike electric field. This occurs in spite of the fact that the pair is *neutral*; i.e., it does not exchange electrons with donors or acceptors possibly present in the sample,

(ii) The Coulomb attraction between charge defects that are created after charge transfer.

(iii) The change in atomic relaxations around the pair compared to those for isolated defects.

As it stems from Table IX, E^{int} ranges from −2.65 to −3.5 eV. In particular, for $V_{\mathrm{Cd}}^{2-}+\mathrm{Zn}_i^{2+}$, $E^{\mathrm{int}}=-2.65$ eV of which (i) the main contribution, −2.1 eV, is provided by transfer of two electrons from Zn_i to V_{Cd}; (ii) electrostatic attraction between the charged defects contributes −0.25 eV; and (iii) additional lattice relaxation upon pairing gives −0.3 eV. Consequently, formation energies of neutral V-I pairs drop to about 1.9 eV in CdTe and to about 2.5 eV in ZnTe; see Table IX and Fig. 11. The calculated electrostatic attraction between the 2− and 2+ point charges spaced by the distance equal to that between V_{Cd} and Zn_i in CdTe is 1 eV, which is higher than the calculated attraction of the V_{Cd}-Zn_i pair due to the delocalized character of changes in the charge density induced by Zn_i and V_{Cd}.

In both CdTe and ZnTe, a FP induces a deep midgap singlet, reminiscent of the singlet induced by an isolated interstitial (Sec. IV). This state is empty in the case of a neutral FP and occupied by one or two electrons for sufficiently high Fermi level. Transition energies between the three charge states are listed in Table IX. The dependence of formation energies on E_F is presented in Figs. 11(a) and 11(b). E_{form} for different charge states is calculated using Eq. (1). For higher E_F we see a reduction in E_{form}, which reflects the acceptor-like character of a FP. As it stems from Figs. 11(a) and 11(b), E_{form} can be reduced to 0.75 eV in CdTe and nearly zero for ZnTe when E_F approaches CBM. The close proximity of defects in the complex and the coupling between them lowers the distance between V and I by 0.4 Å in CdTe and 0.12 Å in ZnTe relative to the ideal configuration. Lowering of the local symmetry from T_d to C_{3v} splits the triplet level of the vacancy into a doublet and a singlet by about 20–30 meV.

The interaction energy E^{int} introduced in Eq. (6) includes the energy gain of charge transfer between I and V, because the reference (i.e., initial) energy is that of the isolated and neutral V and I. However, it is more natural to define the binding energy E_{bind} of a FP as the energy gain due to formation of a FP from isolated V and I for a given Fermi energy, when the defects are in their appropriate charge states:

$$E_{\mathrm{bind}} = E_{\mathrm{form}}[V-I] - E_{\mathrm{form}}[V] - E_{\mathrm{form}}[I]. \tag{7}$$

TABLE IX. The calculated formation energies $E_{\mathrm{form}}(V^0)+E_{\mathrm{form}}(I^0)$ (in eV) of noninteracting neutral defects and the intrapair interaction energies $E^{\mathrm{int}}(V+I)$. Calculated transition energies $\varepsilon(0/-)$ and $\varepsilon(-/--)$ in eV for the FP in CdTe and ZnTe are without M-P correction. The values obtained when including the image charge correction (cf. Sec. IV) are given in parentheses.

	$V_{\mathrm{Cd}}^0+\mathrm{Cd}_i^0$	$V_{\mathrm{Cd}}^0+\mathrm{Zn}_i^0$	$V_{\mathrm{Zn}}^0+\mathrm{Cd}_i^0$	$V_{\mathrm{Zn}}^0+\mathrm{Zn}_i^0$
$E_{\mathrm{form}}(A^0)+E_{\mathrm{form}}(B^0)$	4.69	4.57	5.77	5.45
$E^{\mathrm{int}}(A+B)$	−2.85	−2.65	−3.23	−3.09
$E_{\mathrm{form}}(A+B)$	1.84	1.92	2.54	2.36
$\varepsilon(0/-)$	0.96 (1.07)	0.84 (0.95)	1.03 (1.16)	0.93 (1.06)
$\varepsilon(-/--)$	1.30 (CBM+0.03)	1.24 (1.57)	1.35 (1.74)	1.30 (1.69)

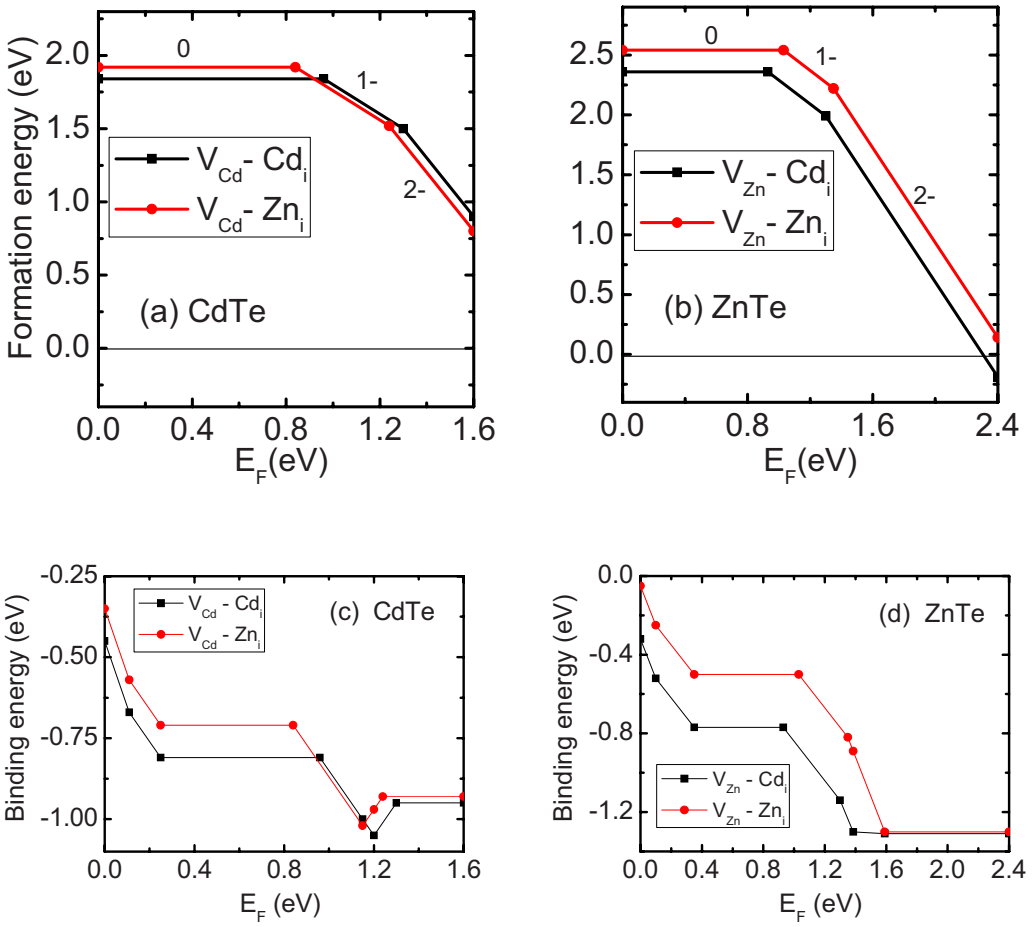

FIG. 11. (Color online) Calculated dependencies on the Fermi energy of (a) formation energies of V_{Cd}+Cd_i and V_{Cd}+Zn_i in CdTe and (b) V_{Zn}+Cd_i and V_{Zn}+Zn_i in ZnTe, and of the binding energies of FPs in (c) CdTe and (d) ZnTe.

The binding energy E_{bind} includes not only the Coulomb coupling and changes in the local lattice relaxation, but also the electronic structure of the defects. The calculated binding energies shown in Figs. 11(c) and 11(d) display a relatively complex dependence on E_F, because this is E_F that determines the charge states of V, I, and the FP, and thus the effective coupling.

The dependence of E_{bind} on the Fermi level is schematically explained in Fig. 12. According to Eq. (7), E_{bind} is defined by the difference in formation energies of a FP relative to that of the isolated V and I, which are sketched in Figs. 12(a)–12(c). For the sake of transparency, the intracenter Coulomb interactions are neglected, and thus V may assume only the 2− and 0 charge states, and both I and FP, the 0 and 2− states. The dependence of E_{bind} on E_F [Fig. 12(d)] stems from the relative positions of the levels of the defects. The possible values of E_F span the band gap and are split into four segments bound by the values of E_F, at which one of the defects changes its charge state. The respective charge states are shown in Fig. 12(e). In particular, region B corresponds to the case of an intrinsic sample, when V and I are in the 2− and 2+ charge states, respectively. For higher E_F, in segment C, formation of the FP lowers the total energy because the (occupied) level of the FP is lower than that of the isolated I. In the opposite case the total energy would rise.

The nonvanishing binding energies together with the mobility of Zn_i and Cd_i imply a tendency to form V-I pairs. In n-type samples, cation vacancies are the dominant compensating acceptors, and their concentration exceeds that of interstitials. Thus, most interstitials should form V-I pairs, but a finite concentration of isolated and nonpaired vacancies is expected. The situation is reversed in p-type samples, where the interstitials are the dominant compensating donors, their concentration is higher than that of vacancies, and thus a finite concentration of isolated interstitials is expected.

VIII. CONDUCTIVITY SWITCHING AND POLARIZATION EFFECTS: A MICROSCOPIC MODEL

Experimental results on conductivity switching and polarization effects can be summarized as follows:

(1) Schottky diodes based on CdZnTe,[5,50] CdZnS,[7] CdZnSe,[9] and CdMnTe (Ref. 8) exhibit resistive bistability, i.e., reversible changes in resistivity between low- and high-resistance states induced by sufficiently high external voltages. Depending on the system, conductivities in these states differ from 2 to 6 orders of magnitude. They are due to the changes in carrier concentration and not in their mobility.

(2) II–VI alloys in high resistive state reveal ferroelectric behavior, i.e., the presence of electric polarization with a

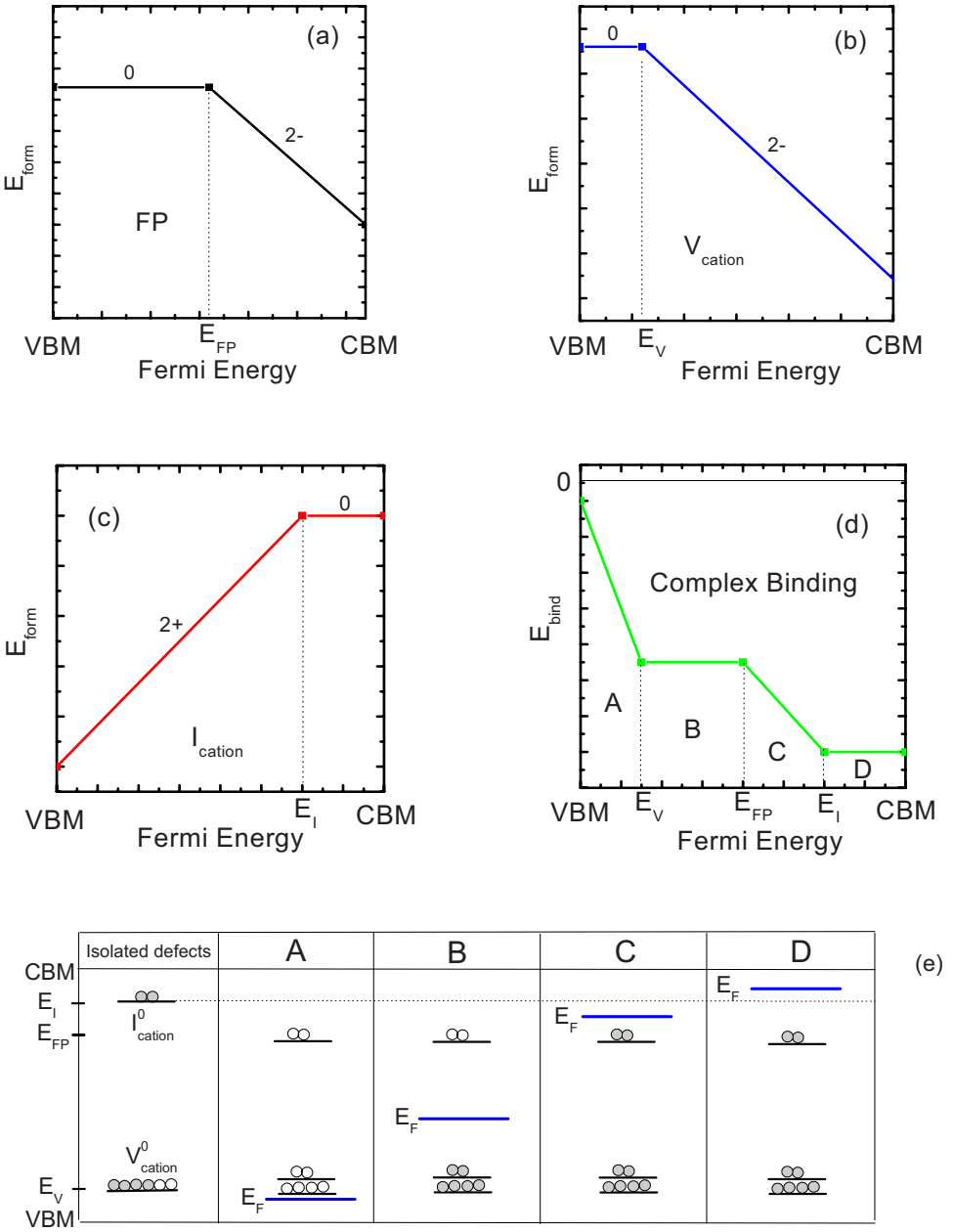

FIG. 12. (Color online) Schematics of defect formation energies E_{form} of (a) a Frenkel pair, (b) an isolated cation vacancy V_{cation}, and (c) an isolated cation interstitial I_{cation} as a function of the Fermi level. The circles mark transition energies. (d) Binding energy E_{bind} of the FP obtained as the difference between E_{form} of the FP with respect to those of the isolated I_{cation} and V_{cation}. E_{bind} can be divided into four characteristic regions of E_F, denoted as A, B, C, and D, in which the charge states of the defects differ, as shown in (e).

hysteresis loop.[4,5,11,50,51] Polarization can be altered by free carriers generated by illumination of samples.[5]

(3) Conductivity switching and ferroelectric behavior are observed only in alloys and are absent in the end binary compounds.[50,51] For example, the effect is observed in CdZnTe with the Zn content ranging from 4% to about 30%, but not in CdTe nor in ZnTe.[11,50]

(4) CdZnTe alloys have an undistorted zinc-blende structure, as shown recently by synchrotron-radiation diffraction[13] and x-ray diffraction.[50]

(5) Polarization effects in CdZnTe are observed both in bulk samples and in epitaxial layers, and both in intrinsic and *p*-type samples, which indicates that the effects have an intrinsically bulk character.[10,50]

(6) Current-voltage characteristics and ferroelectric hysteresis is asymmetric in crystalline samples and symmetric in polycrystalline samples.[10]

(7) Optical spectra of CdZnTe are different in the two resistivity states.[52]

Bistabilities of conductivity and electric polarization were previously observed in Schottky diodes based on the ferroelectric semiconductor $PbTiO_3$.[53] In this system, the intrinsic electric field of $PbTiO_3$ contributes to the total field in the

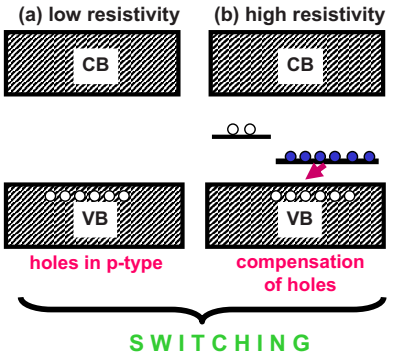

FIG. 13. (Color online) Scheme of the electronic structure of CdZnTe. (a) Low-resistivity situation: *p*-type CdZnTe with holes in the valence band. No defects are present. (b) High-resistivity situation: after the generation of V_{cation}-Zn_i pairs, the holes are compensated by electrons from the defect states.

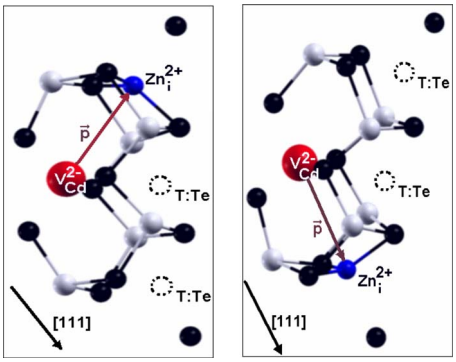

FIG. 14. (Color online) Two configurations of a V_{cation}-Zn_i pair in CdZnTe. Cd and Te atoms are represented by white and black spheres, respectively. Dotted circles indicate possible interstitial T:Te sites. Left and right figures correspond to two different orientations of the electric dipole of the FP.

diode. Interpretation of experiment is based on the fact that a reversal of ferroelectric polarization induces changes in the width of the depletion zone, and thus switches the diode between the high- and the low-conductivity states. The observed electrical characteristics of diodes based on II–VI alloys strongly resemble those of ferroelectric diodes. However, the zinc-blende structure of II–VI alloys prohibits ferroelectricity, and thus a different explanation is to be found. Clearly, it is not possible to provide a detailed interpretation of all experimental results at this stage, since this would require both a more complete experimental understanding of physical processes and a simulation of conductivity of diodes at the mesoscopic scale, which is outside the scope of this paper. However, the results obtained here allow us to tentatively propose that the experimental data listed above stem from the generation-recombination of *V-I* pairs.

In particular, generation of FPs may explain conductivity switching in CdZnTe diodes. The scenario is schematically shown in Fig. 13. Initially, the junction is in the low-resistivity state, since free carriers are present and concentrations of possible compensating defects are negligible. When the applied voltage is high, the induced electric field causes bending of bands and accumulation of electrons at the appropriate interface. The presence of excess electrons induces in turn generation of FPs, as it is discussed in Sec. VII and shown in Fig. 13(b). In this situation, partially occupied states exist in the gap, and electrons from the defect states may compensate for free holes and switch the system to the high-resistivity state. This process is shown for a *p*-type layer, but the possibility of compensation of *n*-type layers is also evident. FPs may recombine, which brings the system back to the low-resistivity state [Fig. 13(a)]. This model also explains why the observed optical spectra in the low- and the high-resistance states are different, ascribing the effect to presence of defects in the latter case.

The presence of FPs is also a possible source of electric polarization and its changes. In fact, electric polarization and its hysteresis are observed in samples in the high-resistivity state, in which, according to the proposed model, there is a finite concentration of FPs. Since V_{cation} is a double acceptor and Zn_i is a double donor, after formation of the complex, two electrons are transferred from the interstitial to the vacancy, which corresponds to the formation of an electric dipole shown in Fig. 14. According to the results in Sec. V, diffusion of a positively charged Zn_i^{++} occurs by long jumps between two adjacent T:Te sites with a barrier of about 0.85 eV. A similar barrier is expected to separate various configurations shown in Fig. 14, in which the interstitial is located at T:Te. In the presence of external electric field, dipoles align along the field direction, and a change in the direction of the field induces a reconfiguration of the dipoles. However, since there are energy barriers between different configurations, a hysteresis of polarization is expected, in agreement with observations.

The proposed model requires a relative stability of FPs, which otherwise would recombine. Stability of FPs is discussed in Sec. VII, where we point out that in general there are finite barriers for recombination of 0.45–0.60 eV (for CdTe:Zn in different charge states). These values are at least twice higher than the barriers of 0.2 eV calculated for metastable *DX*-like configurations of anion vacancies in ZnO and CdTe, which were proposed to cause persistent effects at room temperature.[40] Similarly, it was proposed that the barrier of 0.32 eV stabilizes metastable *DX* centers in Cu(In,Ga)Se_2 up to 300 K.[54] Finally, since the diffusion barrier of 0.2 eV is sufficient to prevent annealing of FPs in Si up to 150 K,[55] one may expect that the barriers of about 0.5 eV should stabilize FPs in CdZnTe at room temperature.

As it was already mentioned, the switching effects are observed only in alloys. This fact was recently confirmed by a detailed experimental study of CdZnTe.[50] The results in Sec. VII A are in qualitative agreement with this observation. First, the barrier for generation of a V_{cation}-Zn_i pair is the lowest; see Figs. 8 and 9 and Table VIII. Second, this pair is the only stable one in all accessible charge states. For the remaining FPs in the +1 state assumed in *p*-type samples the barrier for recombination is lower than 0.1 eV, or vanishes; see Fig. 8 and Table VIII. Finally, as it follows from Fig. 6(a), the barrier for the jump to the next stable site of Zn_i^{2+} is about 0.85 eV, which is relatively high and thus stabilizes the V_{cation}-Zn_i pair with respect to dissociation. In contrast, in the case of V_{cation}-Cd_i [Fig. 6(b)], both the T:Te and the T:Cd

sites are almost equivalent, and therefore this pair may easier dissociate. These three factors may explain why both the conductivity switching and the ferroelectric behavior are observed only in CdZnTe alloys and they are absent in pure ZnTe and CdTe.

Finally, the model implies that in monocrystals both the resistivity switching and the polarization effects are not symmetric when the sign of the applied voltage is reversed, because the formation of the *V-I* pairs occurs along the [111] direction that lacks the reflection plane. This feature agrees with experimental results, which are symmetric only in the case of polycrystalline samples.

To conclude, the proposed microscopic model provides a tentative and qualitative interpretation of experimental observations (1)–(7) summarized in the beginning of this section. However, there are other effects that may affect both the resistivity and the capacitance of diodes based on II–VI alloys, such as the field-driven in-diffusion and electromigration of contaminations from contacts due to the lack of control of interfaces.

IX. SUMMARY

Properties of vacancies, interstitials, and vacancy-interstitial Frenkel pairs in CdTe, ZnTe, and their alloys were studied in detail by calculations within density-functional theory in the generalized gradient approximation. Analysis of generation and stability of Frenkel pairs has revealed their strong dependence on both the sublattice and the Fermi energy. In the case of the cation sublattice, the energy barrier for generation of a FP is reduced from ~ 2.5 eV in intrinsic samples to ~ 1.2 eV in *n*-type samples. Thus, the presence of excess electrons efficiently enhances the pair generation. In particular, a nearest-neighbor pair of cation vacancy-interstitial Zn in CdZnTe alloy is both the easiest to form and relatively stable with respect to the recombination process of the *V-I* defect pair. In contrast, energy barriers for formation of *V-I* pairs on the anion sublattice are about 5 eV independent of E_F, which makes this process highly nonefficient. The position of the Fermi level has also a surprisingly large effect on the binding energy of the vacancy-interstitial pair.

A comprehensive interpretation of formation energies, electronic structure, and diffusion of cation interstitials is provided. Various aspects of the physics of interstitials, such as (i) their stable locations in the crystal, (ii) dependence of the stable location on both the defect charge state and the energy structure of the host semiconductor, and (iii) heights of energy barriers for diffusion and the character of diffusion "jumps" are found to be largely determined by energies of interstitial-induced gap states, and by their occupation with electrons. The calculated energy barriers of Cd_i and Zn_i in both CdTe and ZnTe depend on the charge state of the interstitial and in general are low, about 0.6 eV, which implies their efficient diffusion.

Finally, the obtained results allow proposal of a tentative microscopic interpretation of recent experimental data on electrical bistability and ferroelectric effects observed in Schottky diodes based on CdZnTe and other II–VI alloys. In this model, the switching between the low- and the high-conductivity states is ascribed to the generation of *V-I* Frenkel pairs, which act as compensating centers (explaining the transition to the high-resistivity state), centers attracting excitons (explaining optical properties), and microscopic dipoles that give rise to macroscopic electric polarization. The dependence of the generation of FPs on the Fermi energy is an important ingredient of the model. Thus, the mechanism underlying bistabilities in II–VI alloys is different from that operating in Schottky diodes based on ferroelectric semiconductors.[53]

ACKNOWLEDGMENTS

The authors thank G. Karczewski and T. Wojciechowski for many stimulating discussions. The calculations were done at the Interdisciplinary Centre for Mathematical and Computational Modeling at Warsaw University and at CINECA thanks to HPC-EUROPA grant.

[1] T. E. Schlesinger, J. E. Toney, H. Yoon, E. Y. Lee, B. A. Brunett, L. Franks, and R. B. James, Mater. Sci. Eng., R. **32**, 103 (2001).
[2] R. Muller, S. De Jonge, K. Myny, D. Wouters, J. Genoe, and P. Heremans, Appl. Phys. Lett. **89**, 223501 (2006); R. Müller, R. Naulaerts, J. Billen, J. Genoe, and P. Heremans, *ibid.* **90**, 063503 (2007).
[3] Y. Arimoto and H. Ishiwara, MRS Bull. **29**, 823 (2004).
[4] R. Weil, R. Nkum, E. Muranevich, and L. Benguigui, Phys. Rev. Lett. **62**, 2744 (1989).
[5] D. J. Fu, J. C. Lee, S. W. Choi, S. J. Lee, T. W. Kang, M. S. Jang, H. I. Lee, and Y. D. Woo, Appl. Phys. Lett. **81**, 5207 (2002).
[6] L. Benguigui, R. Weil, E. Muranevich, A. Chack, E. Fredj, and A. Zunger, J. Appl. Phys. **74**, 513 (1993).
[7] P. van der Sluis, Appl. Phys. Lett. **82**, 4089 (2003).
[8] D. J. Fu, J. C. Lee, S. W. Choi, C. S. Park, G. N. Panin, T. W. Kang, and X. J. Fan, Appl. Phys. Lett. **83**, 2214 (2003).
[9] L. Benguigui, R. Weil, E. Muranevich, A. Chack, and E. Fredj, J. Appl. Phys. **74**, 513 (1993).
[10] I. Stolichnov, E. Colla, N. Setter, T. Wojciechowski, E. Janik, and G. Karczewski, Phys. Rev. Lett. **97**, 247601 (2006).
[11] Y. Hotta, E. Rokuta, H. Tabata, H. Kobayashi, and T. Kawai, Appl. Phys. Lett. **78**, 3283 (2001).
[12] A. Marbeuf, C. Mondoloni, R. Triboulet, and J. Rioux, Solid State Commun. **75**, 275 (1990).
[13] Y. Yoneda, N. Matsumoto, K. Suzuya, S. Kohara, and J. Mizuki, Ferroelectrics **268**, 277 (2002).
[14] S.-H. Wei, S. B. Zhang, and A. Zunger, Phys. Rev. Lett. **70**, 1639 (1993).
[15] Y.-C. Chang, R. B. James, and J. W. Davenport, Phys. Rev. B **73**, 035211 (2006).
[16] M. A. Berding, Phys. Rev. B **60**, 8943 (1999).
[17] S.-H. Wei and S. B. Zhang, Phys. Rev. B **66**, 155211 (2002).

[18] P. Hohenberg and W. Kohn, Phys. Rev. **136**, B864 (1964).
[19] W. Kohn and L. J. Sham, Phys. Rev. **140**, A1133 (1965).
[20] J. P. Perdew, J. A. Chevary, S. H. Vosko, K. A. Jackson, M. R. Pederson, D. J. Singh, and C. Fiolhais, Phys. Rev. B **46**, 6671 (1992).
[21] J. P. Perdew, K. Burke, and M. Ernzerhof, Phys. Rev. Lett. **77**, 3865 (1996).
[22] S. Baroni, A. Dal Corso, S. de Gironcoli, and P. Giannozzi (http://www.pwscf.org).
[23] D. Vanderbilt, Phys. Rev. B **41**, 7892 (1990).
[24] D. Vanderbilt (http://www.physics.rutgers.edu/~dhv/uspp/).
[25] M. Methfessel and A. T. Paxton, Phys. Rev. B **40**, 3616 (1989).
[26] H. J. Monkhorst and J. D. Pack, Phys. Rev. B **13**, 5188 (1976).
[27] G. Henkelman and H. Jonsson, J. Chem. Phys. **113**, 9978 (2000); G. Henkelman, B. P. Uberuaga, and H. Jonsson, *ibid.* **113**, 9901 (2000).
[28] P. Pulay, Chem. Phys. Lett. **73**, 393 (1980).
[29] C. Kittel, *Introduction to Solid State Physics* (Wiley, New York, 1996).
[30] M. J. Kirton, P. W. Bank, L. D. Lian, and M. Jaros, J. Phys. C **17**, 2487 (1984).
[31] T. Soma, J. Phys. C **11**, 2669 (1978).
[32] W. A. Harrison, *Electronic Structure and Properties of Solids* (Freeman, San Francisco, 1980).
[33] C. Persson, Y.-J. Zhao, S. Lany, and A. Zunger, Phys. Rev. B **72**, 035211 (2005).
[34] Y. Bar-Yam and J. D. Joannopoulos, Phys. Rev. B **30**, 1844 (1984).
[35] C. G. Van de Walle and J. Neugebauer, J. Appl. Phys. **95**, 3851 (2004).
[36] G. Makov and M. C. Payne, Phys. Rev. B **51**, 4014 (1995).
[37] See, e.g., G. B. Bachelet, G. A. Baraff, and M. Schluter, Phys. Rev. B **24**, 4736 (1981).
[38] M. S. Hybertsen and S. G. Louie, Phys. Rev. Lett. **55**, 1418 (1985).
[39] A. Janotti and Chris. G. Van de Walle, J. Cryst. Growth **287**, 58 (2006).
[40] S. Lany and Alex Zunger, Phys. Rev. B **72**, 035215 (2005).
[41] P. Boguslawski and J. Bernholc, Phys. Rev. B **56**, 9496 (1997).
[42] J. Lento, J.-L. Mozos, and R. M. Nieminen, J. Phys.: Condens. Matter **14**, 2637 (2002).
[43] M. J. Puska, S. Poykko, M. Pesola, and R. M. Nieminen, Phys. Rev. B **58**, 1318 (1998).
[44] G. M. Dalpian and Su-Huai Wei, Phys. Rev. B **72**, 075208 (2005).
[45] T. M. Duc, C. Hsu, and J. P. Faurie, Phys. Rev. Lett. **58**, 1127 (1987).
[46] J. C. Bourgoin and J. W. Corbett, in *Lattice Defects in Semiconductors*, IOP Conf. Proc. No. 23, edited by F. A. Huntley (Institute of Physics, Bristol, 1975), p. 149.
[47] S. B. Zhang, S.-H. Wei, and A. Zunger, J. Appl. Phys. **83**, 3192 (1998).
[48] S. Lany, H. Wolf, and T. Wichert, Phys. Rev. Lett. **92**, 225504 (2004).
[49] J. Dabrowski and M. Scheffler, Phys. Rev. Lett. **60**, 2183 (1988); D. J. Chadi and K. J. Chang, *ibid.* **60**, 2187 (1988); **61**, 873 (1988).
[50] T. Wojciechowski, E. Janik, E. Dynowska, K. Fronc, and G. Karczewski, Phys. Status Solidi C **3**, 1197 (2006).
[51] Y. Hotta, E. Rokuta, J.-H. Jhoi, H. Tabata, H. Kobayashi, and T. Kawai, Appl. Phys. Lett. **80**, 3180 (2002).
[52] T. Wojciechowski, P. Jakubas, P. Bogusławski, and G. Karczewski (unpublished).
[53] P. W. M. Blom, R. M. Wolf, J. F. M. Cillessen, and M. P. C. M. Krijn, Phys. Rev. Lett. **73**, 2107 (1994).
[54] S. Lany and Alex Zunger, Phys. Rev. Lett. **100**, 016401 (2008).
[55] M. J. Beck, L. Tsetseris, and S. T. Pantelides, Phys. Rev. Lett. **99**, 215503 (2007).